Monthly Notices
of the
ROYAL ASTRONOMICAL SOCIETY

MNRAS **428,** 563–572 (2013) doi:10.1093/mnras/sts055

A massive bubble of extremely metal-poor gas around a collapsing Lyα blob at $z = 2.54$

A. Humphrey,[1,2]⋆ L. Binette,[3,4] M. Villar-Martín,[5] I. Aretxaga[2] and P. Papaderos[1]

[1]*Centro de Astrofísica da Universidade do Porto, Rua das Estrelas, 4150-762 Porto, Portugal*
[2]*Instituto Nacional de Astrofísica, Óptica y Electrónica, Luis Enrique Erro 1, Sta. Ma. Tonantzintla, Puebla, México*
[3]*Instituto de Astronomía, Universidad Nacional Autónomo de México, Ap. 70-264, 04510 México D.F., México*
[4]*Département de Physique, de Génie Physique et d'Optique, Université Laval, Québec, QC G1V 0A6, Canada*
[5]*Centro de Astrobiología (INTA-CSIC), Carretera de Ajalvir, km 4, 28850 Torrejón de Ardoz, Madrid, Spain*

Accepted 2012 September 20. Received 2012 September 20; in original form 2012 August 9

ABSTRACT

Using long-slit optical spectroscopy obtained at the 10.4 m Gran Telescopio Canarias, we have examined the gaseous environment of the radio-loud quasar TXS 1436+157 ($z = 2.54$), previously known to be associated with a large Lyα nebula and a spatially extended Lyα-absorbing structure. From the Lyα nebula, we measure kinematic properties consistent with infall at a rate of ∼10–100 $M_\odot$ yr^{-1} – more than sufficient to power a quasar at the top of the luminosity function.

The absorbing structure lies outside of the Lyα nebula, at a radius of $\gtrsim$40 kpc from the quasar. Against the bright unresolved continuum and line emission from the quasar, we detect in absorption the N V λλ1239, 1241, C IV λλ1548, 1551 and Si IV λλ1394, 1403 doublets, with no unambiguous detection of absorption lines from any low-ionization species of metal. The metal column densities, taken together with the H I column density measurement from the literature, indicate that the absorbing gas is predominantly ionized by the quasar, has a mass of hydrogen of $\gtrsim 1.6 \times 10^{11}$ $M_\odot$, a gas density of $\leq$18 cm^{-3}, a line-of-sight thickness of $\geq$18 pc and a covering factor approaching unity. While this absorbing structure is clearly not composed of pristine gas, it has an extremely low metallicity, with ionization models providing a 3σ limit of 12+log(O/H) $\leq$ 7.3.

To explain these results, we discuss a scenario involving starburst-driven superbubbles and the creation of infalling filaments of cold gas which fuel/trigger the quasar. We also discuss the possibility of detecting large-scale absorbers such as this in emission when illuminated by a powerful quasar.

Key words: galaxies: active – galaxies: evolution – galaxies: ISM – quasars: absorption lines – quasars: emission lines – quasars: individual: TXS 1436+157.

1 INTRODUCTION

Lyα nebulae at high redshift ($z \gtrsim 2$; HzLAN), sometimes also known as Lyα 'blobs', 'haloes' or 'fuzz', are prodigious sources of H I Lyα photons, with luminosities up to ∼10^{45} erg s^{-1} and sizes often exceeding ∼100 kpc (e.g. Steidel et al. 2000). HzLANs are not associated with a common type of galaxy; they are variously associated with ultraviolet (UV)-selected star-forming galaxies, dusty star-forming galaxies, powerful active galactic nuclei (AGN) or with no apparent optical galaxy at all (e.g. McCarthy et al. 1987; Reuland et al. 2003; Webb et al. 2009; Steidel et al. 2011; Bridge et al. 2012).

A complete understanding of the nature of HzLANs has not yet been reached, with key properties such as their dominant power source(s) and their space density remaining particularly poorly understood. Nevertheless, HzLANs are thought to represent an important phase of mass assembly, and understanding this energetic phenomenon promises to yield significant insights into the physics of massive galaxy formation (e.g. Mori & Umemura 2006).

Associated absorbers offer a complementary means by which the gaseous environment of galaxies can be studied (e.g. Pettini et al. 2002; Fosbury et al. 2003; Wilman et al. 2005). A substantial fraction of radio-loud, powerful active galaxies at high z show spatially extended, narrow [full width at half-maximum (FWHM) $\lesssim$ 500 km s^{-1}] absorption lines, usually H I Lyα, close to the redshift of the galaxy; the observational characteristics of the absorbers

⋆ E-mail: andrew.humphrey.mexico@gmail.com

suggest that they are giant shells of gas, with radii $\gtrsim$50 kpc, and are distinct structures from the narrow line-emitting nebulae that are also usually associated with powerful active galaxies (Röttgering et al. 1995a; van Ojik et al. 1997; Binette et al. 2000; Jarvis et al. 2003; Wilman et al. 2004; Humphrey et al. 2008a). Intriguingly, in the case of high-z radio galaxies there is a strong anticorrelation between the projected size of the radio source and the detection of associated H I absorbers, with ∼90 per cent of high-z radio galaxies that have small radio sources (<50 kpc) showing an associated absorber, falling to ∼25 per cent for large radio sources (>50 kpc; van Ojik et al. 1997). This result has been interpreted in terms of (a) creation of an expanding shell of gas swept up from the interstellar medium (ISM) of the host galaxy by the expanding radio source (e.g. Krause 2002) or (b) pre-existing gaseous shells produced by powerful starbursts, which are overtaken and disrupted by the expanding radio source (e.g. Jarvis et al. 2003). It is not yet clear whether the absorbing shells are in infall or outflow (e.g. Jarvis et al. 2003; Humphrey et al. 2008a). At least a few of the H I absorbers also contain carbon, as shown by their detection in C IV λ1549 absorption lines (e.g. Binette et al. 2000; Jarvis et al. 2003; Humphrey et al. 2008a). Binette et al. (2000, 2006) and Jarvis et al. (2003) have used ionization models to place important constraints on the metallicity, the source of ionization and the density of the H I and C IV absorbers detected in front of radio galaxies USS 0200+015 ($z = 2.23$) and USS 0943−242 ($z = 2.92$). Interestingly, Vernet et al. (2001) detected various narrow absorption lines from low-ionization or neutral species of C, O, S and Si against the UV continuum emission of several high-z radio galaxies, and noted a tendency for the absorption lines to be stronger in the galaxies with more highly polarized UV continuum emission. The possible relationship between these low-ionization metal absorption lines and the spatially extended H I absorbers is not yet clear.

Quasars provide a useful alternative perspective from which we may examine narrow associated absorbers. The relatively unobscured view to their highly luminous central engines significantly enhances the detectability of narrow absorption lines that would, as in type II quasars or radio galaxies, otherwise lie in spectral regions with no strong continuum or line emission. The absorbers also ought to have a relatively unobscured view of the AGN, raising the possibility that some of the narrow absorbers associated with quasars may be photoionized by the hard radiation field of the AGN; this may result in the detection of absorption lines from more numerous metal species than neutral or stellar-photoionized absorbers, greatly aiding analyses of excitation and metallicity. Moreover, by examining the properties of associated absorbers as a function of AGN and jet orientation, information about the geometry of the absorbers can be obtained. Indeed, Baker et al. (2002), in their study of associated absorption in radio-loud quasars, found that the detection of associated narrow C IV absorbers is orientation dependent, being detected more frequently in the lobe-dominated or steep spectrum quasars than in the flat-spectrum or core-dominated quasars, suggesting that the absorbing gas lies away from the axis of the radio jet. The authors also noted an anticorrelation between the equivalent width of narrow C IV absorption lines and the projected diameter of the radio source, broadly similar to the trend identified by van Ojik et al. (1997) for high-z radio galaxies.

We have begun a programme of spectroscopic observations, designed to help elucidate the nature of Lyα nebulae and H I absorbers associated with powerful active galaxies at high z. By targeting active galaxies known to show extended Lyα nebulae, extended H I absorption close to the redshift of the galaxy, and a very bright unresolved emission component ($\gtrsim 10^{-17}$ erg s cm^{-2} Å^{-1}), we aim to obtain the geometric, ionization and chemical properties of individual absorbers. This approach also mitigates some problems inherent to previous studies, such as the lack of sufficiently bright background emission to readily detect absorption lines other than H I Lyα or C IV, or the lack of an extended background source to provide information about the size and location of the absorber. Based on this idea, Humphrey et al. (2008a) employed deep long-slit spectroscopy from Keck II, together with integral field spectroscopy from the Very Large Telescope, to examine the properties of a spatially extended H I absorber associated with the reddened radio-loud quasar MRC 2025−218. The authors traced the H I absorption feature across a projected area of ∼30 kpc × 40 kpc, with very little variation in kinematic properties therein, which implies the absorber is a coherent structure located at least 20 kpc from the AGN. Against the unresolved continuum and line emission from the active nucleus, narrow absorption lines of C I, C II, C IV, N V, O I, Si II, Si IV, Al II and Al III were detected at the redshift of the H I absorber. The relative column densities of the metal absorption lines indicate that the absorbing gas is photoionized by the active nucleus, has a gas density of $\gtrsim$10 cm^{-3} and is enriched in metals.

Following on from Humphrey et al. (2008a), in this paper we present long-slit spectroscopic observations obtained at the 10.4 m Gran Telescopio Canarias (GTC) of the $R = 19.6$ quasar TXS 1436+157 at $z = 2.537$. With a 4.7 GHz flux density of 47 mJy, this quasar qualifies as radio loud, and its radio source shows a steep spectrum and a lobe-dominated morphology (Röttgering 1993; Carilli et al. 1997). Of particular relevance to this programme, TXS 1436+157 is also known to be embedded within an ∼90 kpc diameter nebula with a Lyα luminosity of $\geq 2.2 \times 10^{44}$ erg s^{-1} (Röttgering et al. 1997; van Ojik et al. 1997), and shows a strong and spatially extended Lyα absorption feature within its Lyα emission line profile (van Ojik et al. 1997). The primary aim of this paper is to elucidate the properties and origins of the Lyα nebula and the associated absorber. We assume $H_0 = 71$ km s^{-1} Mpc^{-1}, $\Omega_\Lambda = 0.73$ and $\Omega_m = 0.27$. At the redshift of TXS 1436+157, 1 arcsec corresponds to 8.2 kpc.

2 OBSERVATIONS AND DATA REDUCTION

Long-slit spectroscopic observations of TXS 1436+157 were obtained in service mode on 2010 May 16 and 21, using the Optical System for Imaging and low Resolution Integrated Spectroscopy instrument at 10.4 m GTC. The observing conditions were dark and photometric. The total integration of 7590 s was split into three integrations of 2530 s each, one of which was carried out on 2010 May 16, while the other two were carried out on 2010 May 21. Although the FWHM of the seeing disc was 1 arcsec during all of the observations, the primary mirror segments were not optimally aligned, which resulted in a poor spatial point spread function *along the slit* (FWHM = 2.3, 1.6 and 2.3 arcsec). The R1000B grism was used, yielding a spectral range of 3700–7000 Å. A 1.23 arcsec wide slit was used and was oriented at a position angle of 140° north through east, so as to include TXS 1436+157 and three additional sources that are within ∼30 arcsec of the quasar, and which are closely aligned with the major axis of the quasar's radio emission (Röttgering et al. 1995). Fig. 1 shows our 20 s acquisition image taken through a Sloan r filter, with the slit position overlaid. The instrument was read-out with 2 × 2 binning, resulting in a spatial scale of 0.25 arcsec pixel^{-1} and a wavelength scale of 2.22 Å pixel^{-1} The data were reduced in the standard way using the long-slit reduction software from the IRAF software suite. Flux calibration was performed using observations of GRW+708247.

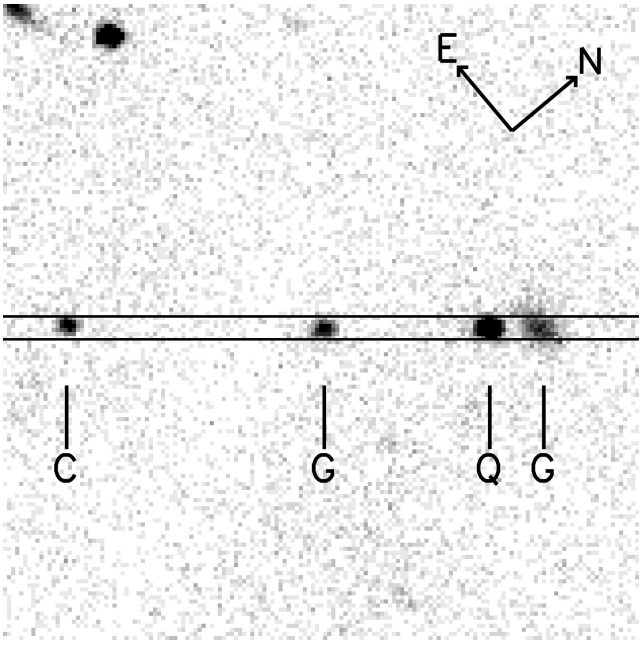

Figure 1. Image of the 40 arcsec × 40 arcsec field around TXS 1436+157, taken through a Sloan *r* filter with an exposure time of 20 s. The position of the long slit is shown. Four discrete sources were within the slit: the $z = 2.54$ quasar TXS 1436+157 (Q); two galaxies which we know now to be at $z = 0.160$ and 0.159 (G); and a continuum only source of unknown redshift (C).

Since the slit width (1.23 arcsec) was significantly larger than the seeing disc FWHM (∼1 arcsec), the instrumental profile (IP) differs between unresolved and extended sources. For extended sources the FWHM of the IP is 11.0 Å, measured from night sky lines in the spectra; this IP will be adopted when calculating the FWHM of emission lines from spatially extended line-emitting gas. For unresolved sources, it is expected to be ∼8 Å, in good agreement with narrow emission lines in the spectra of the intervening star-forming galaxies and from the strong absorption lines in the spectrum of the quasar; this IP will be used for absorption lines detected against the unresolved line and continuum emission of the quasar.

3 INTERLOPING SOURCES

The broad-band image of TXS 1436+157 presented by Röttgering et al. (1995b) shows four tightly aligned sources, including the active galaxy, running along a position angle of ∼140° (see our Fig. 1). The radio source shows a roughly similar position angle (Carilli et al. 1997). Our long slit was positioned so as to encompass all four of these sources, in order to investigate the nature of these aligned optical sources. Our long-slit spectrum reveals that the two closest sources on the sky to TXS 1436+157 are in fact emission line galaxies at intermediate redshift. At a distance on the sky of 3 arcsec NW, SDSS J143904.77+153121.5 has $z = 0.159$, while SDSS J143905.47+153112.6 at a distance of 11 arcsec SE has $z = 0.160$. Thus, the alignment of these nearby (in projection) sources with the radio source is merely coincidental. In the case of the source 25 arcsec to the SE, we do not detect any strong absorption or emission features, and thus we cannot ascertain its redshift.

4 RESULTS AND DISCUSSION

4.1 Measuring equivalent width for absorption lines

For a formal detection, we require (i) that the FWHM of the candidate absorption feature is not smaller than that of the IP, (ii) that the difference between the continuum level and the minimum of the feature is at least twice the local 1σ pixel-to-pixel uncertainty in flux density and (iii) in the case of doublets, that the wavelength separation and relative equivalent width (W_λ) are in agreement with their theoretical values. Since they are doublets and satisfy criterion (iii), our identifications of the N V, Si IV and C IV lines are rather secure ($>10\sigma$). Due to the low spectral resolution of the data, absorption lines were measured using single negative Gaussian profiles, in order to obtain their W_λ. Uncertainties are derived from uncertainty in the level of the underlying continuum and broad line emission.

The C IV absorption doublet has altered the overall velocity profile of the C IV line to such an extent that the velocity profile of the unabsorbed emission, and hence W_λ, cannot reliably be reconstructed – at least at this spectral resolution (Fig. 2). Our determined lower limit on W_λ was measured assuming that the two emission peaks of the C IV profile represent the maximum height of the intrinsic (unabsorbed) line profile. The velocity profile of H I Lyα presents a similar challenge at our spectral resolution. In this case, we refer to the moderate-resolution spectrum and fitting presented by van Ojik et al. (1997), who favoured $N_{\rm H\,I} \sim 4.0 \times 10^{19}$ cm^{-2}.

Table 1 lists the detected absorption lines. Velocities are given relative to the centroid of the narrow He II λ1640 emission at the position of the quasar. Fig. 2 shows regions of the extracted one-dimensional spectrum around the detected N V, Si IV and C IV absorption lines. Table 1 also includes upper limits for several potentially useful absorption lines. These limits were determined by calculating the equivalent width that would correspond to a Gaussian absorption feature that has an FWHM equal to that of the appropriate IP (8 Å), and a minimum that is below the continuum level by at least twice the local 1σ pixel-to-pixel uncertainty in flux density.

The approximate expected wavelength of the O I λ1302.2 line coincides with a detected absorption line at ∼4606 Å, but the presence of an absorption feature at this wavelength in the spectra of the two intermediate-redshift star-forming galaxies (Fig. 3) suggests that it may instead be due to an absorption system in front of all three galaxies (i.e. at $z \lesssim 0.16$). Therefore, we adopt the equivalent width of this absorption line as an upper limit to that of O I λ1302.2. In Fig. 4, we illustrate the conspicuous absence of various other low-ionization absorption lines.

4.2 Column densities using the CoG

We use the curve of growth (CoG) method to derive column densities from the observed values of W_λ (Spitzer 1978). First, we must ascertain on which part of the CoG are the absorption lines. For the two clearly resolved doublets N V λλ1239, 1241 and Si IV λλ1394, 1403, the ratio between the equivalent widths of the blue and red line, $W_{\rm blue}/W_{\rm red}$ can be used. $W_{\rm blue}/W_{\rm red} = 2.0$, 1.1 or $\sqrt{2}$, for the linear, flat or damping parts of the CoG, respectively. For the N V doublet, $W_{\rm blue}/W_{\rm red} = 2.1\pm0.5$ places it on the linear part of the CoG. In the case of the Si IV doublet, the measured $W_{\rm blue}/W_{\rm red} = 1.6\pm0.6$ is ambiguous. However, if we assume that the Si IV lines have a similar intrinsic width to the N V lines, then the fact that $W_{\rm Si\,IV} \sim W_{\rm N\,V}$ would place the Si IV lines on the linear part of the CoG also.

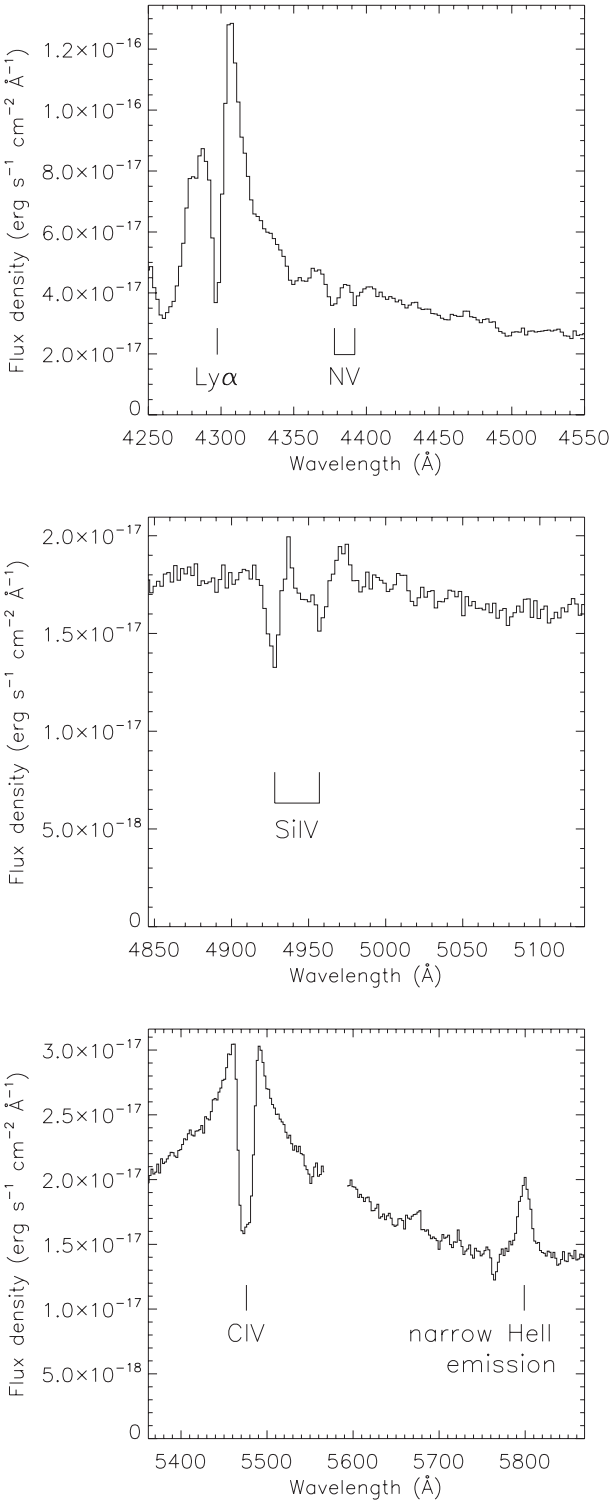

Figure 2. Sections of the one-dimensional spectrum showing the absorption lines detected in front of TXS 1436+157. In the lower panel, the gap in the data between C IV and He II hides a substantial sky-subtraction residual.

For an absorption line on the linear part of the CoG, the column density N can be calculated using

$$N = \frac{1.13 \times 10^{20} W_{\lambda,0}}{f\lambda_0{}^2}, \quad (1)$$

Table 1. Measurements and limits for the absorption lines. Columns: (1) species; (2) rest-frame wavelength (Å); (3) velocity shift (km s^{-1}) relative to the central wavelength of the nuclear narrow He II λ1640 emission line; negative values indicate a blueward shift; the 1σ uncertainties are 50–70 km s^{-1}; (4) observer-frame equivalent width (Å); we show for completeness the lower limit, for C IV; (5) oscillator strength of the transition(s); (6) column density of the species. The rows beginning with 'N V mean' and 'Si IV mean' give $1/\sigma^2$-weighted means for $N_{\rm NV}$ and $N_{\rm SiIV}$, respectively. 'Si II total' gives a combined upper limit for the 1260.4 Å line and the 1264.7 Å excited fine structure line.

Species	λ_0 (Å)	Δv (km s^{-1})	W_λ (Å)	f	N (10^{14} cm^{-2})
(1)	(2)	(3)	(4)	(6)	(7)
H I	1215.7	−70 [a]			∼4 × 10^5 [a]
C I, C I*	1561.1		≤0.2	0.080	≤0.33
C I, C I*	1657.2		≤0.4	0.14	≤0.33
C II, C II*	1335.3		≤0.7	0.13	≤1.0
C IV	1549.5	−220	≥8.4	0.29	≥3.8
N V	1238.8	−190	1.9±0.2	0.16	2.47±0.26
N V	1242.8	−120	0.9±0.2	0.078	2.39±0.53
N V mean					2.45±0.23
O I	1302.2		≤1.2	0.049	≤4.6
Mg I	2026.5		≤0.6	0.11	≤0.42
Si I	1425.0		≤0.3	0.19	≤0.25
Si I	1845.5		≤0.3	0.23	≤0.12
Si II	1260.4		≤0.9	1.18	≤0.15
Si II*	1264.7		≤0.6	1.18	≤0.10
Si II total			≤1.5		≤0.25
Si IV	1393.8	−40	3.1±0.3	0.52	0.98±0.09
Si IV	1402.8	−170	1.9±0.7	0.26	1.19±0.44
Si IV mean					0.99±0.09
S I	1807.3		≤0.6	0.11	≤0.52
S II	1259.5		≤0.6	0.016	≤7.5

[a]The H I velocity and column density are taken from van Ojik et al. (1997).

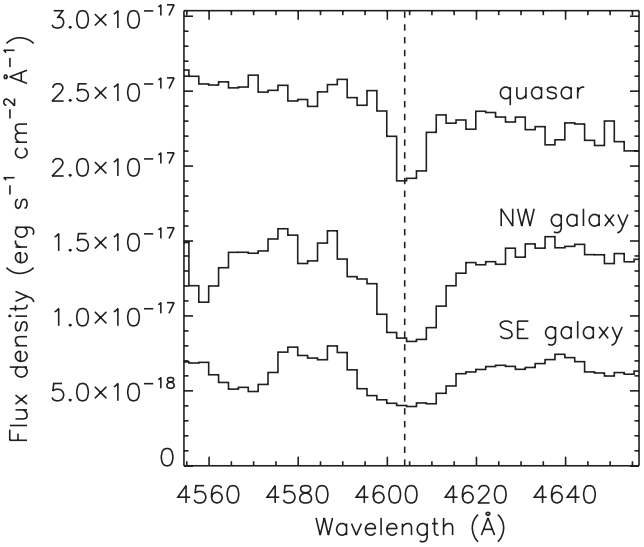

Figure 3. Sections of the one-dimensional spectra of TXS 1436+157 and the two intervening H II galaxies, with the expected wavelength of the O I λ1302.2 absorption line marked with a dashed line. The flux scale is for TXS 1436+157; the spectra of the intervening galaxies have been scaled up and smoothed. Note that all three of the galaxies show a strong absorption feature close to this wavelength.

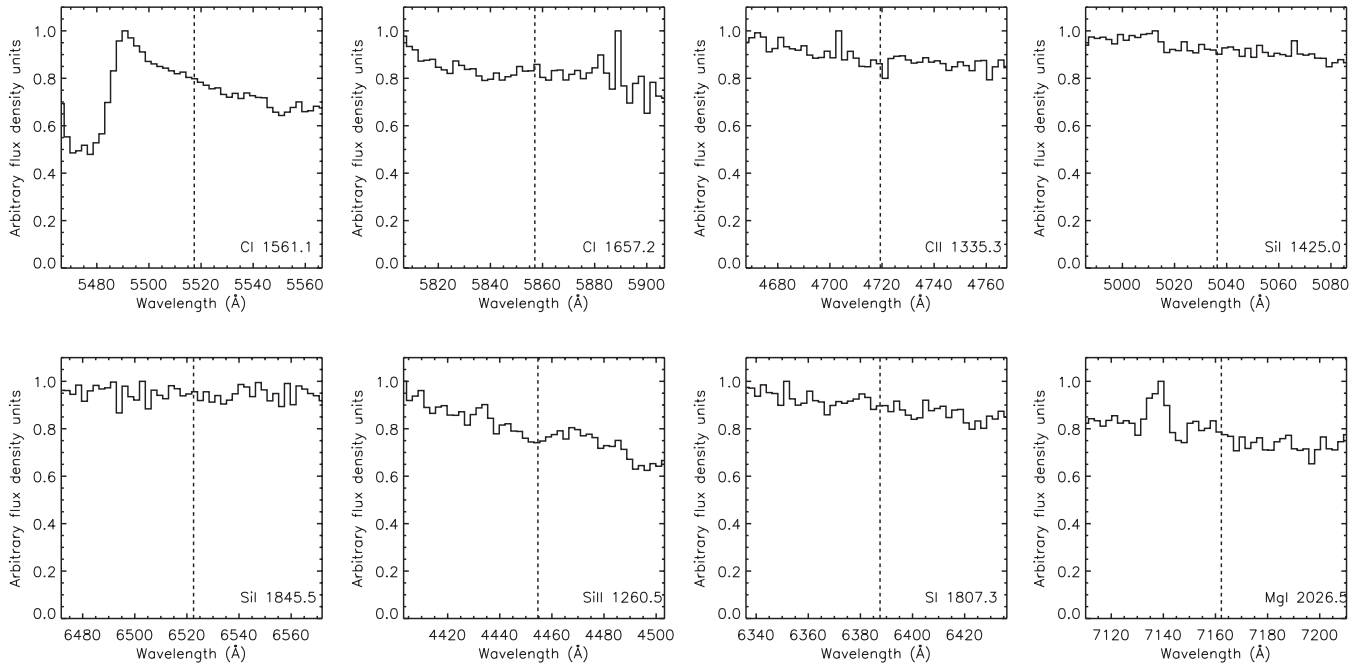

Figure 4. Sections of the one-dimensional spectrum of TXS 1436+157 showing the expected wavelengths of various undetected low-ionization lines. The flux scale is arbitrary, and no smoothing has been performed. Upper limits on W_λ are given in Table 1.

where f is the oscillator strength, $W_{\lambda,0}$ is the rest-frame equivalent width (in Å), λ_0 is the rest-frame wavelength of the line (in Å) and N is in units of cm^{-2}. The resulting σ^{-1}-weighted column densities are $N_{\rm N\,V} = 2.45 \pm 0.23 \times 10^{14}$ and $N_{\rm Si\,IV} = 0.99 \pm 0.09 \times 10^{14}$ cm^{-2}. For C IV we apply this relation to our lower limit to $W_{\rm C\,IV}$ to obtain a lower limit $N_{\rm C\,IV} \geq 3.8 \times 10^{14}$ cm^{-2}.

4.3 Properties of the absorber

4.3.1 Metallicity and ionization

What can be said about the absorber independently of photoionization models? The detection of metal absorption lines from ionized species clearly demonstrates that the absorber is not composed of pristine material. Moreover, it must be at least partially ionized, with the detection of the N V doublet signalling photoionization by a hard radiation field with a significant photon luminosity at $h\nu \geq 77.5$ eV ($\lambda \leq 160$ Å). Given that $N_{\rm C\,IV}/N_{\rm C\,I} + N_{\rm C\,II} \geq 3.0$ and $N_{\rm Si\,IV}/N_{\rm Si\,I} + N_{\rm Si\,II} \geq 2.7$, we can say that the absorber must be predominantly ionized.

In order to further investigate the ionization and chemical composition of the absorber, we have computed photoionization models using the code MAPPINGS IC (Binette, Dopita & Tuohy 1985; Ferruit et al. 1997). We adopt an ionizing spectral energy distribution appropriate for a powerful quasar, characterized by a power law with spectral index $\alpha = -1.5$ (e.g. Robinson et al. 1987; this is justified by the detection of N V absorption lines). The hydrogen density is set to $n_{\rm H} = 10$ cm^{-3}. In the low-density regime, using a different value does not significantly affect the model results. We adopt an isochoric behaviour for the gas density. We take the ionization parameter[1] U to vary from 0.0001 to 1.6 in steps of a factor of 2. We adopt the solar abundances of Anders & Grevesse (1989), except in the case of oxygen for which we adopt the more recent determination of O/H $= 4.9 \times 10^{-4}$ made by Allende Prieto, Lambert & Asplund (2001). We compute models for four different gas metallicities:[2] $Z = 8.69$ (solar), 7.69 (1/10 solar), 6.69 (1/100 solar) and 5.69 (1/1000 solar). In the interest of simplicity, we scale all metals equally with oxygen. To be consistent with the observations, each model calculation is ended once the H I column density has reached 4×10^{19} cm^{-2}. This means at low U the models have a large neutral zone, while at the very high-U end the models become matter bounded.

van Ojik et al. (1997) found that the absorbing gas is kinematically very quiescent, with a Doppler parameter of 37 ± 20 km s^{-1} measured from the Lyα absorption feature. We have not considered ionization by shocks on account of this kinematic quiescence.

Fig. 5 shows various column density ratios resulting from our photoionization model calculations. We have plotted ratios involving high ionization, low ionization and neutral species in order to break the degeneracy between the metallicity and ionization state. Our lower limits on C IV/C II and Si IV/Si II require $U \gtrsim 0.01$ and $N_{\rm H} \gtrsim 10^{21}$ cm^{-2}. In addition, the position of the absorber relative to the model loci requires extremely low abundances of the relevant metals. More specifically, $12 + \log$ [Si/H] and $12 + \log$ [N/H] are $\lesssim$6.7 ($\lesssim$1 per cent of solar), and $12 + \log$[C/H] $\lesssim$ 6.2 ($\lesssim$0.3 per cent of solar).

The O I/H I ratio gives us the slightly less sensitive limit $12 + \log$[O/H] $\lesssim$ 7.3 ($\lesssim$4 per cent solar).[3] It is interesting to note that this is comparable to (or below) the oxygen abundance in the neutral phase in the haloes of local star-forming dwarf galaxies (e.g. Thuan, Lecavelier des Etangs & Izotov 2005), and also in the warm

[1] We define the ionization parameter as $U = \frac{Q}{4\pi r^2 c n_{\rm H}}$, where Q is the luminosity of ionizing photons of the ionizing source, r is the distance of the absorber from the ionizing source and $n_{\rm H}$ is the hydrogen density at the front face of the gas cloud.

[2] We define metallicity as $Z = 12 + \log$[O/H].

[3] If the absorption feature at 4604 Å were to be purely due to O I λ 1302.2, then Z = 12 + log[O/H] would change from an upper limit to ∼7.3.

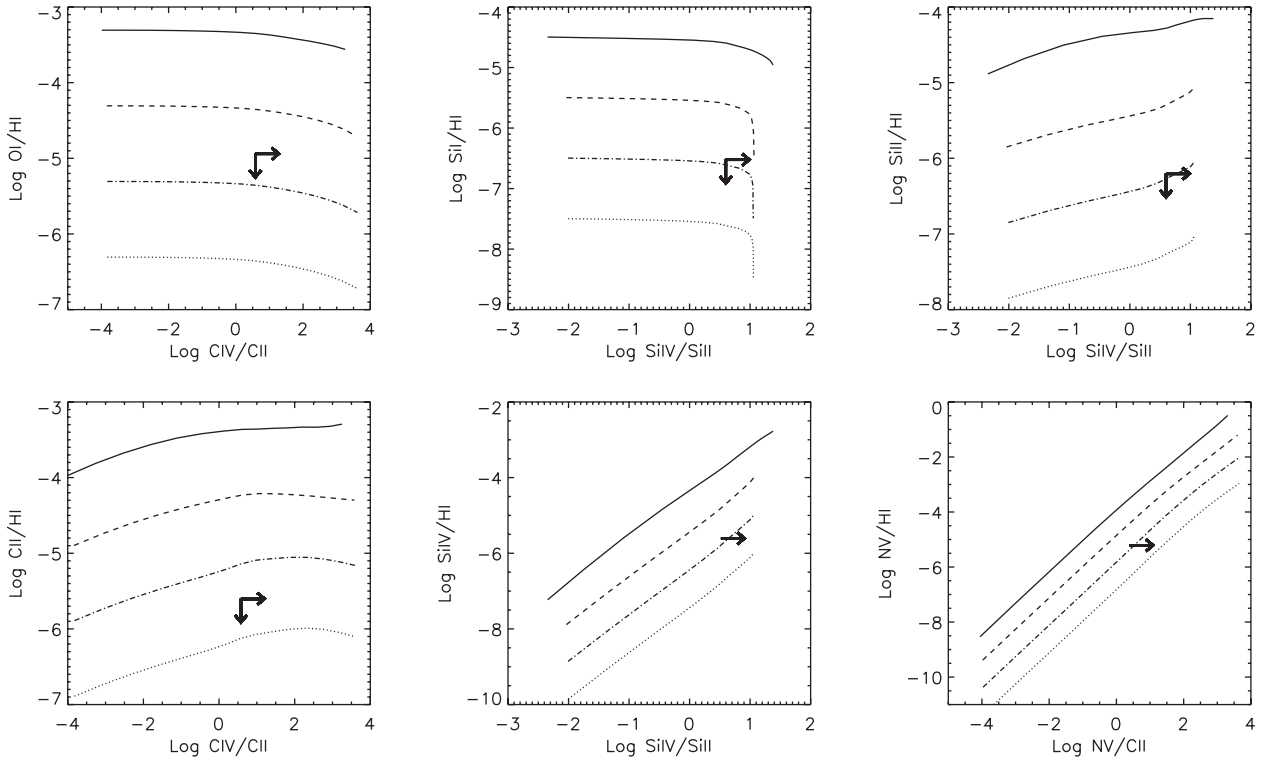

Figure 5. Photoionization model predictions for gas photoionized by an AGN. Each locus represents a sequence in U at four different metallicities (in the 12+log(O/H) system): 8.69 (solid line, solar value), 7.69 (dashed line), 6.69 (dot–dashed line) and 5.59 (dotted line). U increases from the left. Arrows show the measurement or limits on the relevant column density ratios.

ionized phase of extremely metal-poor dwarf galaxies in the nearby Universe (e.g. Izotov et al. 1999, 2006, Izotov et al. 2009; Papaderos et al. 2006).

4.3.2 Geometry and mass

In their moderate-resolution long-slit spectrum of TXS 1436+157, van Ojik et al. (1997) detected the H I Lyα absorption feature out to a projected radius of $\sim$40 kpc from the quasar. This provides us with a rough lower limit of $\gtrsim$40 kpc for the distance of the absorbing structure from the quasar. If the absorbing gas is arranged in a spherical shell with radius $r \geq 40$ kpc encircling TXS 1436+157, then its hydrogen mass can be estimated using

$$M_{\rm H} = 4\pi r^2 m_{\rm H} N_{\rm H}. \quad (2)$$

In this case, the total mass of the absorber would be $\geq 1.6 \times 10^{11}\,{\rm M}_{\odot}$. If we assume instead that the absorber is a uniform sheet of gas then its mass would be

$$M_{\rm H} = A m_{\rm H} N_{\rm H}, \quad (3)$$

where A is the total area of the absorber. Assuming that the absorber is as extended perpendicular to the radio axis as it is observed to be along the radio axis ($\sim$80 kpc; van Ojik et al. 1997), then its total hydrogen mass would be $\geq 5.1 \times 10^{10}\,{\rm M}_{\odot}$.

Since we have a lower limit on U ($\gtrsim$0.01) and on the distance r between the quasar and the absorber ($\geq$40 kpc), and assuming that the ionizing photon luminosity of the central AGN is $\leq 10^{57}$ s^{-1} (e.g. Villar-Martín et al. 2002), the density of the absorbing gas can then be constrained using

$$n_{\rm H} = \frac{Q}{4\pi r^2 c U}. \quad (4)$$

Under these assumptions, we obtain an upper limit of $n_{\rm H} \leq 18$ cm^{-3}. The physical thickness of the absorber along our line of sight towards the quasar is given by

$$l = \frac{N_{\rm H}}{n_{\rm H}}, \quad (5)$$

which gives a lower limit of $l \geq 5.6 \times 10^{19}$ cm, or $\geq$18 pc, assuming a volume filling factor of 1. Significantly lower filling factors (originally suggested by van Ojik et al. 1997) do not seem plausible when one considers that the absorber has a covering factor close to unity over several tens of square kiloparsecs.

It is also interesting to estimate the mass of metals contained within the absorber. In our $U \gtrsim 0.1$ models C IV, N V and Si IV all have an ionization fraction of the order of $\sim$0.1, meaning that the total columns of C, N and Si are probably $\gtrsim$3.8, $\sim$2.5 and $\sim 1.0 \times 10^{14}$ cm^{-2}, respectively. Using equation (2), we then obtain C, N and Si masses of $\gtrsim$6, $\sim$4 and $\sim 2 \times 10^5\,{\rm M}_{\odot}$, respectively. If we adopt the solar Si/O abundance ratio, the mass of oxygen would then be $\sim 2 \times 10^6\,{\rm M}_{\odot}$. According to the calculations of Mollá & Terlevich (2012), the production and injection of this mass of oxygen would require the formation of $\sim 10^9\,{\rm M}_{\odot}$ of stars.

4.4 Detectability of absorbing shells in Lyα emission

Would an absorber of the kind associated with TXS 1436+157 be detectable in emission? For a quasar ionizing luminosity $Q \sim 10^{57}$ s^{-1}, a torus opening angle of $\sim 90^{\circ}$, shell radius $\sim$40 kpc and covering factor $\sim$1, the Lyα luminosity of the absorbing shell would be $\sim 3 \times 10^{45}$ erg s^{-1}, comparable to the Lyα luminosity of the extended nebulae photoionized by quasars and radio galaxies. This assumes that the intervening gas in the host galaxy has a low

covering factor and that the shell is thick enough to absorb all incident ionizing photons. In narrow band imaging, such a shell would appear as a pair of diametrically opposed arcs centred on the quasar, each with a Lyα surface brightness of the order of $\sim 10^{-15}$ erg s^{-1} cm^{-2} arcsec^{-2}. Thus, under the right conditions – a luminous enough quasar surrounded by a shell of sufficient thickness and covering factor – a gaseous structure of this kind should indeed be detectable in Lyα emission.

Interestingly, van Ojik et al. (1997) found that the Lyα absorption feature of TXS 1436+157 is not black at its trough, with a residual flux of $\sim 10^{-16}$ erg s^{-1} in that spectral region. This result is qualitatively consistent with the idea of some in situ production of Lyα photons in the absorber, due to its photoionization by the active nucleus, although other possible explanations exist, such as a covering factor of <1.

4.5 Comparison against other extended metal line absorbers

In this section, we compare and contrast the properties of the absorber associated with TXS 1436+157 with the small number of other spatially extended metal line absorbers known to be associated with high-z active galaxies.

A similar analysis to that we have performed has been done for another radio-loud quasar, MRC 2025−218 at $z = 2.63$ which, like TXS 1436+157, shows a spatially extended Lyα absorber seen in front of the galaxy's quasar-photoionized Lyα emitting nebula (LAN) (Humphrey et al. 2008a). In Table 2, we reproduce from Humphrey et al. (2008a) the properties of that absorber. The absorbers of MRC 2025−218 and TXS 1436+157 show remarkably similar N V column densities, which are $3.6 \pm 1.4 \times 10^{14}$ and $2.5 \pm 0.2 \times 10^{14}$ cm^{-2}, respectively, which itself suggest that the two absorber systems have surprisingly similar (total) nitrogen column densities, and a fairly similar $U = \frac{Q}{4\pi r^2 c n_{\rm H}}$. Moreover, both absorbers are predominantly ionized as shown by their large $N_{\rm Si\,IV}/N_{\rm Si\,I}$ and $N_{\rm C\,IV}/N_{\rm C\,I}$ ratios. The limits on their gas density, although pulling in opposite directions, nonetheless permit a similar density of ~ 10 cm^{-3}.

A comparison with the spatially extended metal line absorbers associated with HzRGs ($z \gtrsim 2$) is also interesting. While many HzRGs show spatially extended H I absorption in front of their extended LAN (e.g. van Ojik et al. 1997), only two have also been unambiguously detected in metal lines. In the case of the $z = 2.92$ HzRG MRC 0943−242, Binette et al. (2000) have detected C IV absorption at the redshift of the extended H I absorber, while Jarvis et al. (2003) detected in C IV absorption the extended H I absorber of the $z = 2.23$ HzRG MRC 0200+015. Interestingly, the two HzRGs have almost identical values of $N_{\rm C\,IV}$: $3.8 \pm 0.4 \times 10^{14}$ and $4.9 \pm 0.2 \times 10^{14}$ cm^{-2} for MRC 0943−242 and MRC 0200+105, respectively, which suggest that their absorbers have similar (total) carbon column densities and similar $U = \frac{Q}{4\pi r^2 c n_{\rm H}}$. Compared to these values, the extended absorber in front of MRC 2025−218 has a substantially higher C IV column density of $N_{\rm C\,IV} = 20^{+20}_{-10} \times 10^{14}$ cm^{-2}, while the absorber in front of TXS 1436+157 has $N_{\rm C\,IV} \geq 3.8 \times 10^{14}$ cm^{-2} which is about as high as or higher than the two HzRGs. This relative enhancement of highly ionized species in the extended absorbers associated with the quasars is consistent with the idea that those absorbers are photoionized by a more intense radiation field – presumably that of the quasar.

Table 2. Emission line ratios measured in the extended line-emitting nebula 2.0–3.8 arcsec east of the quasar. For comparison, we also show the values of the ratios from the $z > 2$ radio galaxy (HzRG) average emission line spectrum of Humphrey et al. (2008b).

Ratio	Value	HzRG average
Lyα/He II λ1640	22 ± 4	11.7
N V λ1241/He II λ1640	≤ 0.3	0.3
N V λ1241/C IV λ1549	≤ 0.2	0.5
N V λ1241/Lyα	≤ 0.014	0.04
C IV λ1549/He II λ1640	1.3 ± 0.2	1.8
C IV λ1549/C III] λ1908	4.2 ± 1.5	2.4
C III] λ1908/He II λ1640	0.3 ± 0.1	0.73

4.6 The Lyα nebula

The properties of the extended LAN are qualitatively consistent with the results presented by van Ojik et al. (1997). The extended Lyα emission has FWHM $= 820 \pm 50$ km s^{-1}, shows an excess of flux in its blue wing and is redshifted by 500 km s^{-1} relative to the He II emission at the position of the quasar: these properties are consistent with effects expected due to the strong, spatially extended Lyα absorption on the blue side of the line profile. Our new results are as follows.

4.6.1 Kinematic properties: infall

Out of the UV emission lines detected in the spectrum of TXS 1436+157, the He II λ1640 line is expected to give the most reliable indication of the kinematic properties of the gas in the LAN. As a non-resonant recombination line from helium, it should be the least sensitive overall to absorption, geometry, metallicity or the ionization parameter. In the eastern region of the LAN, the He II line shows a significant redshift of 110 km s^{-1} from the position of the quasar to $\gtrsim 1$ arcsec to the east,[4] and has FWHM $= 460 \pm 40$ km s^{-1}. These properties are consistent with gravitational motion within a massive galaxy and its dark matter halo. The quiescence of the kinematics are surprising given the small size of the radio source (45 kpc; Carilli et al. 1997), which would usually be associated with extreme gas kinematics (FWHM $\gtrsim$ 1000 km s^{-1}; e.g. Best, Röttgering & Longair 2000; Humphrey et al. 2006; Nesvadba et al. 2006). In order to better understand the kinematic properties of the He II line, we must take into consideration orientation effects.

In the standard paradigm for powerful active galaxies, the ionizing radiation of the quasar is collimated into two diametrically opposed ionization cones by an optically thick toroidal structure around the nucleus. In the case of TXS 1436+157, our relatively direct view of the quasar then implies that we are looking through the base of one of the ionization cones. Gas infalling into the host galaxy is caught in the ionizing radiation field of the quasar, and reprocesses ionizing photons into narrow emission lines. Along the line of sight to the quasar, relatively bright line emission from the ionized gas which is relatively closer to the quasar, and which is nearer to the systemic velocity of the galaxy, should dominate over low surface brightness line emission from the infalling gas. However, along lines of sight substantially offset from the position of the quasar, the line emission would be dominated by the infalling gas and will show a relative redshift. If we assume that the He II line at the position of the quasar is emitted close to the systemic

[4] On the west side of the quasar, He II emission was not detected, although this may simply be due to obscuration by the intervening galaxy at $z = 0.159$.

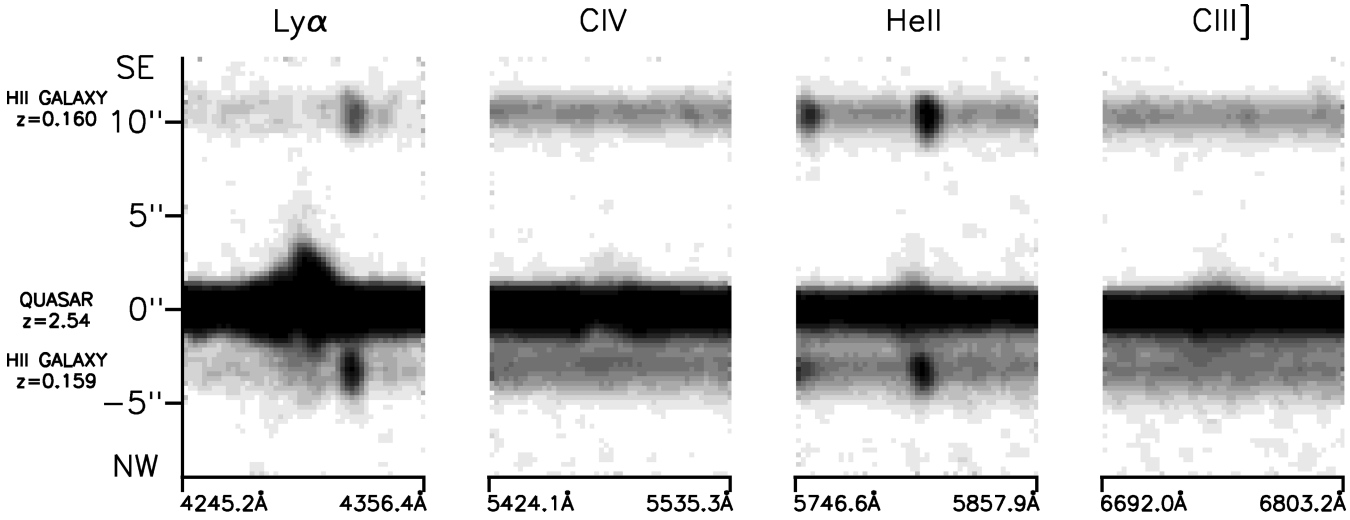

Figure 6. Sections of the two-dimensional spectrum of TXS 1436+157, centred on the brightest narrow emission lines: Lyα, C IV, He II and C III]. The vertical scale is in arcseconds, while the horizontal scale gives observed-frame wavelength in Angstroms. Cut levels are chosen to show the spatially extended, narrow emission lines, and these differ between panels. The data have been smoothed by a 3 pixel box-car average to emphasize the extended line emission.

velocity, then the relative redshift of the line in the eastern LAN indicates that the nebula is in inflow/infall into the host galaxy. This is consistent with previous studies which have concluded that the Lyα nebulae around high-z radio galaxies and quasars often have a significant infalling/inflowing component (Weidinger, Møller & Fynbo 2004; Humphrey et al. 2007; Villar-Martín et al. 2007a).

Only a very rough estimate of the gas infall rate can be obtained from the available information. If we adopt a gas density of $\sim$50 cm^{-2}, a filling factor $\sim 10^{-5}$ (e.g. McCarthy 1993; Villar-Martín et al. 2003) and an infall velocity of 110 km s^{-1} as implied by the velocity redshift of the He II line from the position of the quasar to the east region of the nebula, then the infall rate would be $\sim$10–100 M$_\odot$ yr^{-1}. This is comparable to the gas infall rates estimated by Humphrey et al. (2007) for the giant Lyα nebulae of a sample of radio galaxies at $z > 2$, and is sufficient to power a quasar at the top of the luminosity function ($L_{\rm bol} \sim 10^{46}$ erg s^{-1}).

4.6.2 Excitation: Lyα excess

To measure representative line ratios for the LAN, from our co-added two-dimensional spectrum (shown in Fig. 6), we have collapsed spatially a one-dimensional spectrum from regions at projected distances 2.0–3.8 arcsec east from the position of the quasar. The measurements were done by integrating the total flux above the continuum level, with 1σ uncertainties dominated by the uncertainty in the continuum level. The line ratios are listed in Table 3. The three line ratios formed from only C IV λ1549, He II λ1640 and/or C III] λ1908 are fairly consistent with the $z > 2$ radio galaxy average (Humphrey et al. 2008b; see also McCarthy 1993). The detection of the He II line shows that the LAN is ionized at least in part by the hard radiation field of the quasar, while the detection of the two carbon lines indicate that the gas is enriched in metals. As discussed by Humphrey et al. (2008b) and others, line ratios using only C IV λ1549, He II λ1640 and C III] λ1908 do not provide strong constraints on the metallicity of the emitting gas; metallicities as low as $\sim$5 per cent solar, or as high as a few times solar, are possible for the LAN. However, the non-detection of narrow N V emission argues against very high metallicities (see e.g. Vernet et al. 2001; Humphrey et al. 2008b).

Table 3. Properties of the associated absorber in front of the $z = 2.63$ radio-loud quasar MRC 2025−218, reproduced from Humphrey et al. (2008a). Δv is the velocity shift of the absorber from the velocity centroid of the narrow He II λ1640 emission line measured at the projected position of the quasar.

Species	N (10^{14} cm^{-2})
H I	$\gtrsim$300
C I	1.4 ± 0.3
C II	$\geq$9.9
C IV	20^{+20}_{-10}
N V	3.6 ± 1.4
O I	$\geq$6.8
Si I	$\leq$0.37
Si II	13 ± 11
Si II*	1.7 ± 0.7
Si IV	$\geq$2.6
Al II	$\geq$0.16
Al III	0.4 ± 0.1
Property	Value
r	$\geq$25 kpc
$M_{\rm H}$	$\gtrsim 10^8$ M$_\odot$
$n_{\rm H}$	$\geq$10 cm^{-3}
Δv	-600 km s^{-1}

The Lyα/He II λ1640 ratio, on the other hand, is a factor of $\sim$2 higher than the average value, and is significantly higher than the range of values $\sim$8–15 that 'normal' AGN-photoionization models can produce (Humphrey et al. 2008b). Judging from the fitting carried out by van Ojik et al. (1997) for the extended Lyα emission, the pre-absorbed Lyα flux ought to be a factor of about $\times$ 1.3 higher, which would raise the Lyα/He II ratio to $\sim$29. Lyα excesses of this kind have previously been identified in the LANs of a number of $z > 2$ radio galaxies (e.g. van Ojik et al. 1994; Villar-Martín et al. 2007b), with the previously proposed explanations being (a) cooling radiation from low-metallicity infalling gas, (b) higher than expected nebular temperatures, due to low gas metallicity in the photoionized nebulae, (c) resonance fluorescence or (d) photoionization by young stars (see e.g. Villar-Martín et al. 2007b). In the

case of the Lyα nebula around TXS 1436+157, however, we must discard options (a) and (b) due to the substantial level of chemical enrichment of the nebula, so that only (c) and (d) remain as plausible explanations. Measuring the Lyα/Hα ratio (e.g. Hayashi et al. 2012), or polarimetry of the Lyα emission (e.g. Hayes, Scarlata & Siana 2011), would be useful to distinguish between these possibilities.

4.7 The nature of the absorber and Lyα nebula

Assuming that the narrow He II emission at the position of the quasar is emitted close to the systemic velocity, then the relative blueshift of the absorber implies that it is in outflow. Various previous investigators have discussed the possible origins of similar blueshifted, absorbing structures around HzRGs and quasars (e.g. van Ojik et al. 1997; Binette et al. 2000; Krause 2002; Jarvis et al. 2003; Wilman et al. 2004; Humphrey et al. 2008a). In the case of TXS 1436+157, we favour a scenario adapted from the superbubble scenario devised by Tenorio-Tagle et al. (1999). During a powerful starburst, mechanical energy is deposited by supernovae explosions into the galaxian ISM, producing an expanding superbubble which decelerates as it sweeps up gas from the ISM. The shell becomes Rayleigh–Taylor unstable and fragments (blows out), thereby allowing the thermalized supernovae ejecta to rapidly escape into the low-density halo of the galaxy, which then forms a new expanding shell sweeping up low-metallicity gas from the halo. Left behind from the fragmentation of the initial shell are Rayleigh–Taylor 'fingers' of cooler, denser, metal-enriched gas. These take $\sim$100 Myr to fall from a radius of the order of $\sim$10 kpc into the central regions of the galaxy, at a velocity of $\sim$100 km s^{-1} (see Section 4.6.1), to provide fuel to trigger the quasar and radio jets. The radiation field produced by the quasar then photoionizes the infalling material, thereby allowing its detection in Lyα and other lines, and also provides a background source for detection of the new shell, which has now expanded to a radius of several tens of kpc during the delay between the blow-out event and the triggering of the quasar.

Interestingly, this scenario allows us to reconcile the simultaneous presence of infalling gas with comparatively high metallicity (Humphrey et al. 2007a, 2008b), which would correspond to the Rayleigh–Taylor 'fingers' left behind after the blow-out of the initial shell, and an expanding shell of low-metallicity gas at larger radii (e.g. Binette et al. 2000), corresponding to the second shell of swept-up matter. Naively, one may otherwise have expected gas falling into the galaxy to have substantially lower metallicity than the gas flowing out.

We must also consider whether it is energetically feasible for the expansion of the absorbing shell to be starburst driven. Averaged across the H I, C IV, N V and Si IV lines (Table 1), the current outflow velocity is $\sim$140 km s^{-1}. Assuming that this is a spherical shell of mass $\geq 1.6 \times 10^{11}$ M$_\odot$ (Section 4.3.2), its kinetic energy would then be $\geq 3.1 \times 10^{58}$ erg. This serves as a lower limit on the mechanical energy deposited into the ISM by supernovae. Using fig. 116 of Leitherer et al. (1999), we find that a modest star formation rate of $\sim$20 M$_\odot$ yr^{-1}, over a starburst lifetime of 100 Myr, would be sufficient to produce a mechanical energy luminosity of $\sim 3 \times 10^{58}$ erg. The total mass of stars formed in this starburst would be $\sim 2 \times 10^9$ M$_\odot$, consistent with the stellar mass required to explain the α-element content of the shell (Section 4.3.2).

Powerful radio sources can also provide a source of mechanical energy to potentially drive an outflow (see e.g. Nesvadba et al. 2006; Humphrey et al. 2010). Could the radio source have produced this outflow? The observed radius of the radio source is $\sim$3 arcsec (Carilli et al. 1997). The fact that the radio source shows a relatively small arm-length asymmetry, shows a steep spectrum and is lobe-dominated implies that foreshortening effects on its observed size can be neglected, so that its observed radius then corresponds to $\sim$25 kpc, which is substantially smaller than the $r \geq 40$ kpc of the absorber. While the ionizing radiation field of a quasar can also produce outflows (e.g. Humphrey et al. 2010), the kinetic energy of the shell around TXS 1436+157 is substantially higher than even the most luminous quasars can reasonably inject (e.g. Feruglio et al. 2010). Thus, the expanding shell is unlikely to be driven by either the radio jets or the radiation field of the quasar.

While the results presented in this paper directly concern only a single galaxy, they have wider implications for radio-loud active galaxies. Most radio-loud active galaxies at high z have 10–100 kpc-scale Lyα nebulae (e.g. Heckman et al. 1991; van Ojik et al. 1997) which are infalling where not perturbed by the radio jets (Humphrey et al. 2007). A substantial fraction of these galaxies also show strong H I absorption features against the narrow Lyα emission line, which are usually blueshifted relative to the emission (van Ojik et al. 1997), and whose spatial extension indicates a location outside of the extended Lyα nebula. Clearly, then, TXS 1436+157 is not unique in this regard, and we argue that the scenario we have proposed above should also be applicable to the wider population of high-z, radio-loud active galaxies.

Finally, it is tempting to speculate that the shell may eventually escape from TXS 1436+157 and fragment into smaller self-gravitating baryonic entities, which at a later cosmic epoch may evolve into low-metallicity late-type galaxies. These galaxies would be chemically pre-enriched to a level $12 + \log[\mathrm{O/H}] \sim 7$, in agreement with the low-metallicity threshold empirically found via observations of the most metal-poor star-forming galaxies currently known in the local Universe. Such galaxies would presumably be almost free from dark matter, somewhat analogous to high-metallicity 'tidal dwarf galaxies' ejected from galaxy mergers (see the review by Duc 2010).

5 CONCLUSIONS

Using deep long-slit optical spectroscopy from the 10.4 m GTC, we have investigated the properties of narrow line-emitting and absorbing gas associated with the $z = 2.54$ radio-loud quasar TXS 1436+157. Our main conclusions are as follows.

(i) The large Lyα nebula around the quasar appears to be infalling on to the host galaxy at a rate of $\sim$10–100 M$_\odot$ yr^{-1}. It shows anomalously strong Lyα emission relative to He II λ1640, due to enhancement of Lyα through resonance fluorescence or through photoionization by stars (in addition to by the active nucleus).

(ii) The absorber lies outside of the Lyα nebula and is likely to be a giant expanding shell enclosing the Lyα nebula and the host galaxy. It has a hydrogen mass of $\gtrsim 1.6 \times 10^{11}$ M$_\odot$, a gas density of $\leq$18 cm^{-3}, a geometrical thickness of $\geq$18 pc and a covering factor close to unity.

(iii) The absorber is detected in C IV, N V and Si IV lines, with low-ionization metal lines conspicuously absent, and is photoionized by the quasar. Using photoionization models we conclude that the metallicity of the absorbing gas is $12 + \log[\mathrm{O/H}] \leq 7.3$ – much lower than that of the infalling Lyα nebula. However, the detection of the metal lines shows that this is not pristine material.

(iv) To explain the properties of the Lyα nebula and the absorbing shell, we have proposed a scenario in which a starburst-driven superbubble sweeps up material from the ISM; the bubble ruptures

due to Rayleigh–Taylor instability, leaving behind filaments of cold, metal-enriched gas which fall back into the galaxy to fuel/trigger the quasar, while the hot supernova ejecta flows out into the low-density halo and produces a new, larger shell of swept-up low-metallicity gas.

(v) We argue that when illuminated by a sufficiently luminous quasar, gaseous shells such as this should be detectable in emission lines.

ACKNOWLEDGMENTS

This work is based on observations made during Mexican time with the Gran Telescopio Canarias at the Spanish Observatorio del Roque de los Muchachos, La Palma, Spain. AH acknowledges a Marie Curie Fellowship cofunded by the 7th Research Framework Programme and the Portuguese Fundação para a Ciência e a Tecnologia, and a *CONACyT* post-doctoral research fellowship. AH also acknowledges useful discussions with Patricio Lagos. LB acknowledges support from *CONACyT* grant CB-128556. PP is supported by a Ciencia 2008 contract, funded by FCT/MCTES (Portugal) and POPH/FSE (EC). We also thank the anonymous referee for suggestions that improved this work.

REFERENCES

Allende Prieto C., Lambert D. L., Asplund M., 2001, ApJ, 556, L63
Anders E., Grevesse N., 1989, Geochimica et Cosmochimica Acta, 53, 197
Baker J. C., Hunstead R. W., Athreya R. M., Barthel P. D., de Silva E., Lehnert M. D., Saunders R. D. E., 2002, ApJ, 568, 592
Best P. N., Röttgering H. J. A., Longair M. S., 2000, MNRAS, 311, 23
Binette L., Dopita M. A., Tuohy I. R., 1985, ApJ, 297, 476
Binette L., Kurk J. D., Villar-Martín M., Röttgering H. J. A., 2000, A&A, 356, 23
Binette L., Wilman R. J., Villar-Martín M., Fosbury R. A. E., Jarvis M. J., Röttgering H. J. A., 2006, A&A, 459, 31
Bridge C. R. et al., 2012, arXiv:1205.4030
Carilli C. L., Röttgering H. J. A., van Ojik R., Miley G. K., van Breugel W. J. M., 1997, ApJS, 109, 1
Duc P. A., 2010, inPapaderos P., Recchi S., Hensler G., eds, Proc. JENAM, Dwarf Galaxies: Keys to Galaxy Formation and Evolution. Springer-Verlag, Berlin, p. 305
Ferruit P., Binette L., Sutherland R. S., Pecontal E., 1997, A&A, 322, 73
Feruglio C., Maiolino R., Piconcelli E., Menci N., Aussel H., Lamastra A., Fiore F., 2010, A&A, 518, L155
Fosbury R. A. E. et al., 2003, ApJ, 596, 797
Hayashi M., Kodama T., Tadaki K.-i., Koyama Y., Tanaka I., 2012, ApJ, 757, 1
Hayes M., Scarlata C., Siana B., 2011, Nat, 476, 304
Heckman T. M., Miley G. K., Lehnert M. D., van Breugel W., 1991, ApJ, 370, 78
Humphrey A., Villar-Martín M., Fosbury R., Vernet J., di Serego Alighieri S., 2006, MNRAS, 369, 1103
Humphrey A., Villar-Martín M., Fosbury R., Binette L., Vernet J., De Breuck C., di Serego Alighieri S., 2007, MNRAS, 375, 705
Humphrey A. et al., 2008a, MNRAS, 390, 1505
Humphrey A., Villar-Martín M., Vernet J., Fosbury R., di Serego Alighieri S., Binette L., 2008b, MNRAS, 383, 11
Humphrey A., Villar-Martín M., Sánchez S. F., Martínez-Sansigre A., Delgado R. G., Pérez E., Tadhunter C., Pérez-Torres M. A., 2010, MNRAS, 408, L1
Izotov Y. I., Chaffee F. H., Foltz C. B., Green R. F., Guseva N. G., Thuan T. X., 1999, ApJ, 527, 757
Izotov Y. I., Schaerer D., Blecha A., Royer F., Guseva N. G., North P., 2006, A&A, 459, 71 Izotov Y. I., N. G., K. J., P.,
Izotov Y. I., Guseva N. G., Fricke K. J., Papaderos P., 2009, A&A, 503, 61
Jarvis M. J., Wilman R. J., Röttgering H. J. A., Binette L., 2003, MNRAS, 338, 263
Krause M., 2002, A&A, 386, L1
Leitherer C. et al., 1999, ApJS, 123, 3
McCarthy P. J., 1993, ARA&A, 31, 639
McCarthy P. J., Spinrad H., Djorgovski S., Strauss M. A., van Breugel W., Liebert J., 1987, ApJ, 319, L39
Mollá M., Terlevich R., 2012, MNRAS, 425, 1696
Mori M., Umemura M., 2006, Nat, 440, 644
Nesvadba N. P. H., Lehnert M. D., Eisenhauer F., Gilbert A., Tecza M., Abuter R., 2006, ApJ, 650, 693
Papaderos P., Izotov Y. I., Guseva N. G., Thuan T. X., Fricke K. J., 2006, A&A, 454, 119
Pettini M., Rix S. A., Steidel C. C., Adelberger K. L., Hunt M. P., Shapley A. E., 2002, ApJ, 569, 742
Reuland M. et al., 2003, ApJ, 592, 755
Robinson A., Binette L., Fosbury R. A. E., Tadhunter C. N., 1987, MNRAS, 227, 97
Röttgering H. J. A., 1993, PhD thesis, Leiden Univ.
Röttgering H. J. A., Hunstead R. W., Miley G. K., van Ojik R., Wieringa M. H., 1995a, MNRAS, 277, 389
Röttgering H. J. A., Miley G. K., Chambers K. C., Macchetto F., 1995b, A&AS, 114, 51
Röttgering H. J. A., van Ojik R., Miley G. K., Chambers K. C., van Breugel W. J. M., de Koff S., 1997, A&A, 326, 505
Spitzer L., 1978, Physical Processes in the Interstellar Medium. Wiley-Interscience, New York
Steidel C. C., Adelberger K. L., Shapley A. E., Pettini M., Dickinson M., Giavalisco M., 2000, ApJ, 532, 170
Steidel C. C., Bogosavljević M., Shapley A. E., Kollmeier J. A., Reddy N. A., Erb D. K., Pettini M., 2011, ApJ, 736, 160
Tenorio-Tagle G., Silich S. A., Kunth D., Terlevich E., Terlevich R., 1999, MNRAS, 309, 332
Thuan T. X., Lecavelier des Etangs A., Izotov Y. I., 2005, ApJ, 621, 269
van Ojik R., Röttgering H. J. A., Miley G. K., Bremer M. N., Macchetto F., Chambers K. C., 1994, A&A, 289, 1, p. 54–60
van Ojik R., Röttgering H. J. A., Miley G. K., Hunstead R. W., 1997, A&A, 317, 358
Vernet J., Fosbury R. A. E., Villar-Martín M., Cohen M. H., Cimatti A., di Serego Alighieri S., Goodrich R. W., 2001, A&A, 366, 7
Villar-Martín M., Vernet J., di Serego Alighieri S., Fosbury R., Pentericci L., Cohen M., Goodrich R., Humphrey A., 2002, MNRAS, 336, 436
Villar-Martín M., Vernet J., di Serego Alighieri S., Fosbury R., Humphrey A., Pentericci L., 2003, MNRAS, 346, 273
Villar-Martín M., Sánchez S. F., Humphrey A., Dijkstra M., di Serego Alighieri S., De Breuck C., González Delgado R., 2007a, MNRAS, 378, 416
Villar-Martín M., Humphrey A., De Breuck C., Fosbury R., Binette L., Vernet J., 2007b, MNRAS, 375, 1299
Webb T. M. A., Yamada T., Huang J.-S., Ashby M. L. N., Matsuda Y., Egami E., Gonzalez M., Hayashimo T., 2009, ApJ, 692, 1561
Weidinger M., Møller P., Fynbo J. P. U., 2004, Nat, 430, 999
Wilman R. J., Jarvis M. J., Röttgering H. J. A., Binette L., 2004, MNRAS, 351, 1109
Wilman R. J., Gerssen J., Bower R. G., Morris S. L., Bacon R., de Zeeuw P. T., Davies R. L., 2005, Nat, 436, 227

This paper has been typeset from a TEX/LATEX file prepared by the author.